



Neutronics Assessment of the ITER First Wall/Shield Modules

M.E. Sawan, B. Smith, P. Wilson

June 2007

UWFDM-1326

Presented at the 22nd IEEE/NPSS Symposium on Fusion Engineering, 17-21 June 2007,
Albuquerque NM.

FUSION TECHNOLOGY INSTITUTE

UNIVERSITY OF WISCONSIN

MADISON WISCONSIN

DISCLAIMER

This report was prepared as an account of work sponsored by an agency of the United States Government. Neither the United States Government, nor any agency thereof, nor any of their employees, makes any warranty, express or implied, or assumes any legal liability or responsibility for the accuracy, completeness, or usefulness of any information, apparatus, product, or process disclosed, or represents that its use would not infringe privately owned rights. Reference herein to any specific commercial product, process, or service by trade name, trademark, manufacturer, or otherwise, does not necessarily constitute or imply its endorsement, recommendation, or favoring by the United States Government or any agency thereof. The views and opinions of authors expressed herein do not necessarily state or reflect those of the United States Government or any agency thereof.

Neutronics Assessment of the ITER First Wall/Shield Modules

M.E. Sawan, B. Smith, P. Wilson

Fusion Technology Institute
University of Wisconsin
1500 Engineering Drive
Madison, WI 53706

<http://fti.neep.wisc.edu>

June 2007

UWFDM-1326

Presented at the 22nd IEEE/NPSS Symposium on Fusion Engineering, 17-21 June 2007, Albuquerque NM.

Neutronics Assessment of the ITER First Wall/Shield Modules

M.E. Sawan, B. Smith, and P. Wilson

Fusion Technology Institute, University of Wisconsin, Madison, WI, sawan@engr.wisc.edu

Abstract— Neutronics analysis was performed to support the US design of ITER first wall/shield (FWS) modules 7, 12 and 13. Initial 1-D and 2-D calculations determined nuclear heating radial profiles in each of the constituent materials. In addition, the nuclear parameters were determined at the inner surface of the VV. The impact of radiation streaming through zones with large water content, such as the water coolant manifolds and FW attachment legs, was evaluated. The peaking is largest for nuclear heating that is dominated by gamma heating. Monte Carlo calculations that are directly coupled to the CAD models were utilized to generate high fidelity, high-resolution results for nuclear heating, radiation damage, and helium production.

Keywords—neutronics; ITER; shield modules; nuclear heating; helium production

I. INTRODUCTION

The ITER first wall/shield (FWS) modules consist of a plasma facing first wall (FW) section followed by a shielding section [1]. These modules provide the main thermal and nuclear shielding for the vacuum vessel (VV) and external machine components. The FWS is segmented both in the poloidal and toroidal directions to limit the weight per module to a reasonable weight that can be handled by the remote maintenance equipment. Eighteen (18) modules with different dimensions are arranged in the poloidal direction with the lowest inboard module designated as module 1 and the lowest outboard module designated as module 18. The module toroidal width varies from 1.25 to 1.98 m with the poloidal length varying from 0.85 to 1.24 m. The US is responsible for the design and procurement of modules 7, 12, and 13. The design includes a FW panel assembly that consists of Be armor, Cu heat sink, and steel structure with embedded water coolant tubes. The shield module includes a front steel plate, a front water coolant manifold, a shielding zone with coaxial coolant channels, and a back shield plate. Fig. 1 shows the elements of the FWS module.

The design of the FWS modules includes assessment of the stresses due to nuclear heating and performing detailed computational fluid dynamics (CFD) and electromagnetic (EM) analyses. Accurate calculation of the temperature distribution in the FWS module requires accurate knowledge of the plasma heating of the FW and the volumetric nuclear heating due to neutrons and secondary gamma photons. In addition, re-welding is required at several locations in the FWS module and the VV behind it. This requires accurate determination of helium production in the structural material. Therefore, detailed mapping of nuclear heating, radiation damage, and helium production is an essential input to the design process. In this paper, we present results of the

neutronics analysis performed for the conceptual designs of FWS modules 7, 12, and 13.

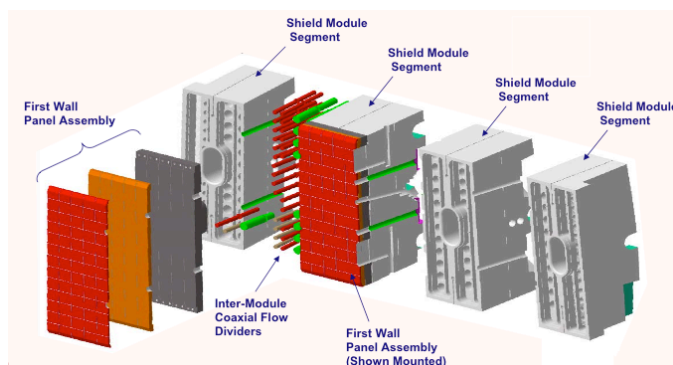


Fig. 1. Elements of the FWS module.

II. NUCLEAR HEATING PROFILES

The neutronics calculations have been performed in steps. We started by performing initial one-dimensional (1-D) calculations using the ONEDANT module of the DANTSYS 3.0 discrete ordinates particle transport code system [2] and the FENDL-2.1 nuclear data library [3]. The calculations used the appropriate radial build and material composition for 8 homogenized radial zones based on the detailed configuration of each module. Due to the curved back of module 7 the thickness varies with the minimum being at the poloidal edges of the module. Two radial builds were used for the thinnest and thickest locations. On the other hand, modules 12 and 13 are uniform in thickness and the same radial build was used in the calculations for both modules. A zone consisting of 65% SS316LN-IG and 35% water is used behind the module to simulate neutron reflection from the VV. We used the detailed elemental composition of the materials of the FWS modules (Be, CuCrZr, SS316LN-IG, and water) as provided by the ITER international organization (IO) [4]. For modules 12 and 13 that are located in the outboard region, we used a toroidal cylindrical geometry model that includes the inboard shielding blanket with its layered configuration to account for proper neutron and gamma reflection. However, for module 7 located at the top of the plasma chamber, a cylindrical geometry with the module radial build fully surrounding the plasma is a more appropriate approximation and was used in the calculations.

The results were normalized to the neutron wall loading at the front of each module. For accurate determination of the neutron wall loading we performed detailed three-dimensional (3-D) calculations for a full ITER CAD model that was developed for ITER neutronics benchmark calculations [5] as shown in Fig. 2. We developed an innovative computational

tool (MCNPX-CGM) that performs the neutronics calculations directly in the CAD model [6,7] and, hence, preserves the geometrical details and eliminates possible human error in modeling. MCNPX-CGM was used in the 3-D calculations of the neutron wall loading. The detailed source profile in the ITER plasma provided by the ITER IO was used in the calculations [8]. For the ITER fusion power of 500 MW, the average neutron wall loadings at the front surfaces of modules 7, 12, and 13 are 0.264, 0.629, and 0.693 MW/m², respectively.

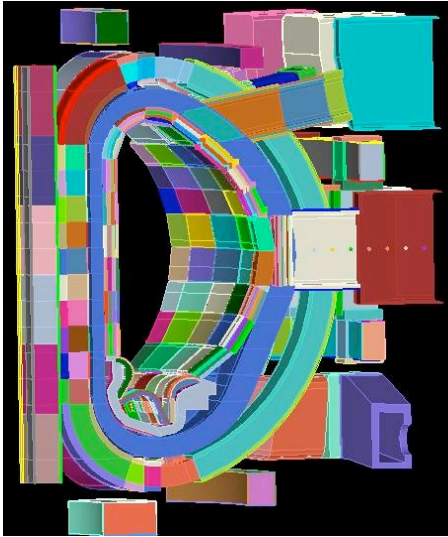


Fig. 2. ITER CAD model used to determine neutron wall loading distribution.

The nuclear heating radial profiles were determined in each of the constituent materials of the FWS modules based on the 1-D calculations. The radial build and homogenized material compositions used for modules 12 and 13 are given in Table I. For module 7 at the thinnest location, the total thickness is 479 mm with the 25 mm difference being in the thickness of zone 7 which has 30% water compared to 25% in modules 12 and 13. Figs. 3 and 4 show the radial variation of nuclear heating in modules 7 and 13, respectively. The peak power densities in Be, CuCrZr, SS, and water of module 7 are 2.9, 4.2, 3.8, and 3.1 MW/cm³, respectively. The corresponding peak values in module 13 are 7.4, 10.9, 8.1, and 8 MW/cm³, respectively. The profiles in module 12 are similar to those in module 13 with values reduced by the ratio of the neutron wall loadings.

Comparing the results for the constituent materials of the FW, it is interesting to note that nuclear heating in CuCrZr is ~10% higher than in SS316LN-IG while that in water is ~20% lower than in SS316LN-IG. There is a flat plateau in the steel heating in the front manifold zone of the shield. This is attributed to the increased amount of gamma generation that dominates steel nuclear heating. The large water content results in softening the neutron energy spectrum leading to more gamma generation in the steel in addition to the larger gamma generation in the water itself.

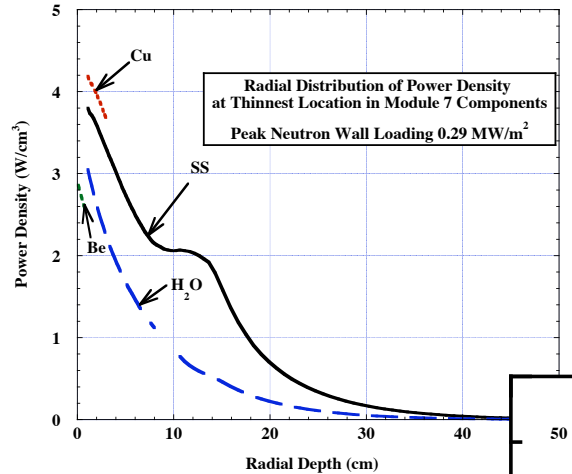


Fig. 3. Radial variation of nuclear heating in module 7.

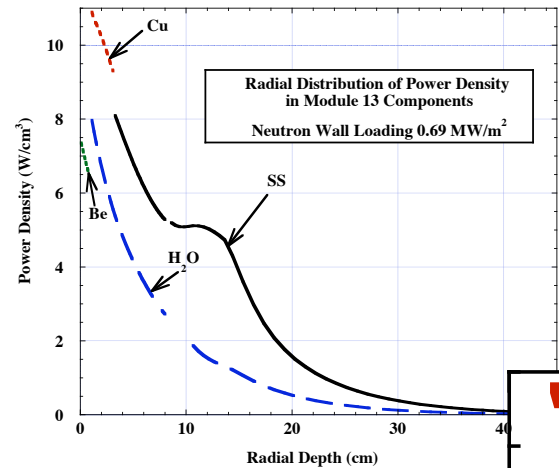


Fig. 4. Radial variation of nuclear heating in module 13.

TABLE I. RADIAL BUILD FOR MODULES 12 AND 13

Zone	Description	Thickness (mm)	% Be	% CuCrZr	% SS316LN-IG	% H ₂ O
1	Be PFC	10	100	0	0	0
2	CuCr Zr heat sink	22	0	82.9	0	17.1
3	SS FW structure	49	0	0	84.6	15.4
4	Gap between FW and shield	3	0	0	0	0
5	Front shield SS plate	20	0	0	100	0
6	Front shield manifold	35	0	0	14	86
7	Bulk of shield module	295	0	0	75	25
8	Back shield SS plate	20	0	0	100	0
Total		454				

III. NUCLEAR PARAMETERS IN VACUUM VESSEL

The nuclear parameters at the front surface of the VV were calculated at the poloidal locations behind FWS modules 7, 12, and 13. The power density, dpa and helium production values in SS316LN-IG are given in Table II. The end-of-life parameters were calculated for the average FW neutron fluence goal of 0.3 MWa/m². It is clear that the cumulative end-of-life helium production is well below the 1 He appm design limit required for re-welding. However, radiation streaming through zones with large water content, such as the water coolant manifolds and FW attachment legs, results in local peaking in the VV radiation parameters.

TABLE II. NUCLEAR PARAMETERS AT FRONT SURFACE OF VV BEHIND FWS MODULES

	Module 7	Module 12	Module 13
Thickness (cm)	47.9	45.4	45.4
Power density (mW/cm ³)	11	34	37
He production rate (appm/s)	1.1x10 ⁻⁹	3.6x10 ⁻⁹	3.9x10 ⁻⁹
End-of-life He appm	0.019	0.061	0.066
dpa rate (dpa/s)	6.5x10 ⁻¹¹	2.0x10 ⁻¹⁰	2.2x10 ⁻¹⁰
End-of-life dpa	0.0011	0.0034	0.0037

Preliminary 1-D neutronics calculations were performed to assess the impact of the poloidal water coolant manifolds on the nuclear parameters in the VV. The calculations used the radial build through the water coolant manifold at poloidal locations corresponding to modules 7, 12, and 13 yielding the results in Table III. These results were compared to those obtained using the nominal FWS module radial build (Table II). The peaking factors in the VV nuclear parameters due to the coolant manifold at the poloidal locations corresponding to modules 12 and 13 are ~1.4-2.5 with the smallest peaking occurring in the dpa rate. The power density, which is dominated by contribution from the gamma photons, exhibits the largest peaking due to the largest gamma generation in water and the softer spectrum at the VV resulting in more gamma generation in the SS316LN-IG itself. The peaking factors at poloidal locations corresponding to module 7 are ~2-3. One should keep in mind that the peaking factor results give conservative estimates for the peaking effect of the manifolds since they are based on 1-D calculations for the manifold radial build with large water content.

TABLE III. NUCLEAR PARAMETERS AT FRONT SURFACE OF VV BEHIND POLOIDAL MANIFOLD AT POLOIDAL LOCATIONS OF MODULES 7, 12, AND 13

	Module 7	Module 12	Module 13
Thickness (cm)	46.4	48.9	48.9
Power density (mW/cm ³)	35	85	93
He production rate (appm/s)	2.2x10 ⁻⁹	5.1x10 ⁻⁹	5.6x10 ⁻⁹
End-of-life He appm	0.038	0.086	0.095
dpa rate (dpa/s)	1.2x10 ⁻¹⁰	2.8x10 ⁻¹⁰	3.0x10 ⁻¹⁰
End-of-life dpa	0.0020	0.0047	0.0050

The FW is attached with a leg that has less thickness and more water content than the shield module. Analysis is needed to determine the effect of streaming through the attachment leg on nuclear heating, radiation damage, and flux peaking in the VV. To quantify this, we developed a 2-D model in r-z geometry that includes the different radial builds used in the attachment leg region (see Table IV) and the shield module 13 region surrounding it. The axis of the cylindrical geometry is coincident with the axis of the FW attachment leg. The main differences are larger water content (~50% in central zone and 90% in front and back zones) in the attachment leg and a ~10 cm gap at its back in front of the VV. The penetration for the leg was represented by a circular region. Two radii (6 cm and 10 cm) were considered to assess the effect of attachment leg size. The TWODANT module of the DANTSYS 3.0 code system was used [2]. The detailed variation of nuclear heating, radiation damage, neutron flux, and gamma flux at the front of the VV was determined as function of distance from the center of the attachment leg.

The variation of nuclear heating, dpa and He production at the front surface of the VV is shown in Fig. 5. The peak nuclear heating in the VV behind a 10 cm radius attachment leg is a factor of ~11 higher than that without the leg. The relative peaking is smaller for radiation damage and gas production. A higher peaking occurs in nuclear heating since it is dominated by gamma heating. The peaking in gamma flux behind the attachment leg is much higher than that in the neutron flux due to the much lower gamma attenuation in water compared to steel. The peaking in VV heating is dominated by the effect of the ~10 cm void zone rather than the increased water content and an effort should be made to reduce the void region behind the attachment leg if possible. We also investigated the impact of leg radius and water content in the central zone of the leg. Reducing the leg size was found to be more effective than reducing the water content.

TABLE IV. RADIAL BUILD FOR FW ATTACHMENT LEG IN MODULE 13

Zone	Description	Thickness (mm)	% Be	% CuCrZr	% SS316LN-IG	% H ₂ O
1	Be PFC	10	100	0	0	0
2	CuCr Zr heat sink	22	0	82.9	0	17.1
3	SS FW structure	49	0	0	84.6	15.4
4	Gap	3	0	0	0	0
5	Front water zone	55	0	0	10	90
6	Central zone of leg	120	0	0	53 (68)	47 (32)
7	Back water zone	98	0	0	10	90
8	Gap	97	0	0	0	0
Total		454				

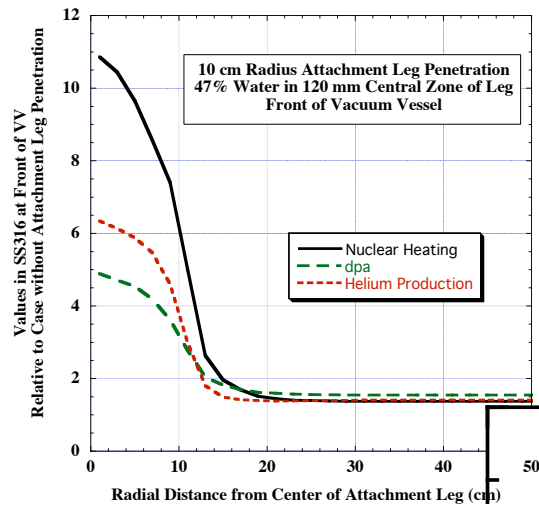


Fig. 5. Peaking in VV nuclear parameters due to FW attachment leg.

IV. HYBRID 1-D/3-D ANALYSIS

In order to capture the impacts of the significant heterogeneity of the FWS module shown in Fig. 1, a hybrid 1-D/3-D neutronics analysis was performed for Module 13. Fundamentally, this model places the 3-D representation of Module 13 into a 1-D model to approximate the coupling to the full machine. Consistent with 1-D modeling of tokamak systems, a cylindrical coordinate system is used, with the central axis of the cylindrical coordinate system aligned with the central axis of the tokamak system. In this model, shown in Fig. 6, homogenized radial regions are included to represent the inboard FWS and outboard VV. The extents of the model in the azimuthal and vertical directions are only large enough to accommodate the module 13 geometry. Reflecting boundary conditions approximate the full extent of ITER in

the poloidal and toroidal directions. While a 1-D model would contain a homogenized approximation of the outboard FWS module, this model includes a full 3-D CAD model for module 13 created at Sandia National Laboratories. A 14.1 MeV uniform source between the inboard and outboard sides is used to simulate the ITER plasma. Results are normalized to a neutron wall loading of 0.693 MW/m^2 calculated using a 3-D model of ITER with a detailed plasma source as discussed in Section II.

The calculations were performed using the MCNPX-CGM code [6,7]. Cartesian mesh tallies were used to provide high fidelity 3-D heating, radiation damage, and helium generation profiles through module 13. These nuclear responses were calculated on $0.5 \text{ cm} \times 0.5 \text{ cm} \times 1 \text{ cm}$ meshes. Figs. 7, 8, and 9 show nuclear heating, SS atomic displacements (dpa), and SS helium production on a surface 11.5 cm from the front of the FW (within the front manifold), with 17 million source particles sampled. It is important to note that the dpa He production results represent the nuclear response to stainless steel when subjected to the neutron flux at each point. Therefore, these values shown in the regions that are actually filled with water are not physically valid but give indication of the level expected in a region with large water content. These are representative of the radiation damage and gas production in the steel T-flow drivers in the front water manifolds. Mesh-based weight windows were used for variance reduction leading to statistical uncertainties $<5\%$. Additional visualizations of the results have been developed to permit a more integrated view of the variations. Fig. 10 provides a visualization of the nuclear heating throughout the front part of the FWS. It clearly shows the variation of nuclear heating due to geometrical changes and attenuation as one moves from the front of the FW deeper into the FWS module.

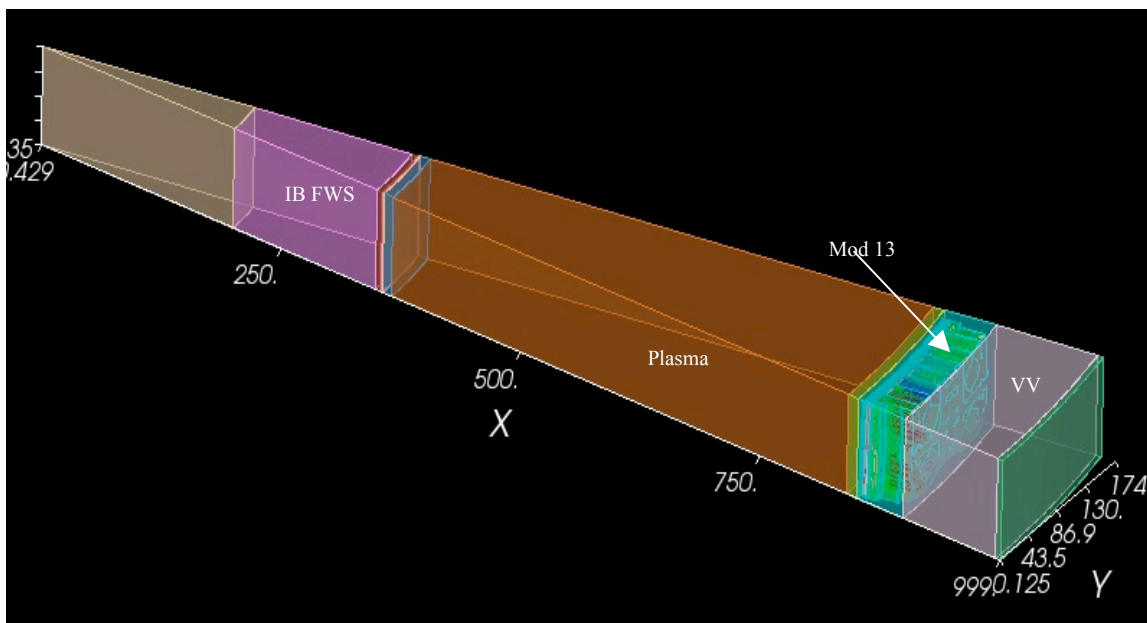


Fig. 6. Hybrid 1-D/3-D model.

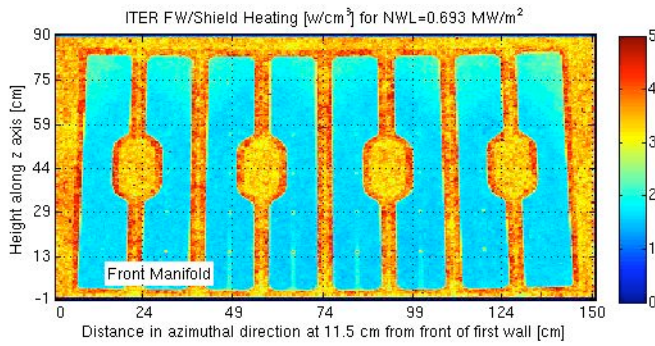


Fig. 7. Nuclear heating distribution in the front manifold region.

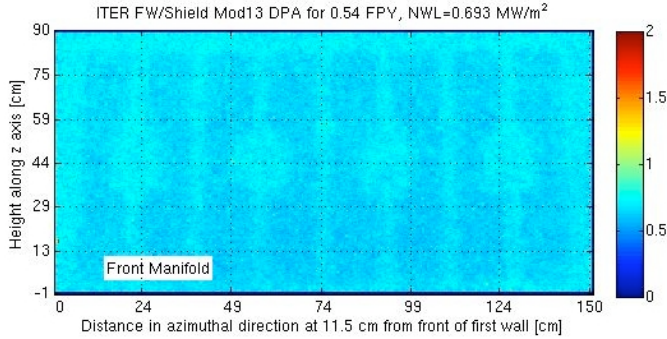


Fig. 8. Steel dpa after 0.3 MWa/m² in the front manifold region.

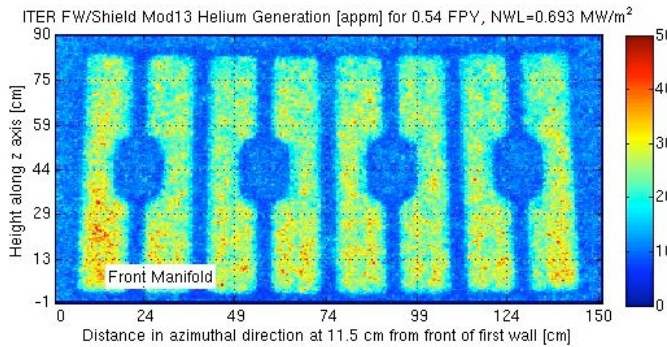


Fig. 9. Steel He production after 0.3 MWa/m² in the front manifold region.

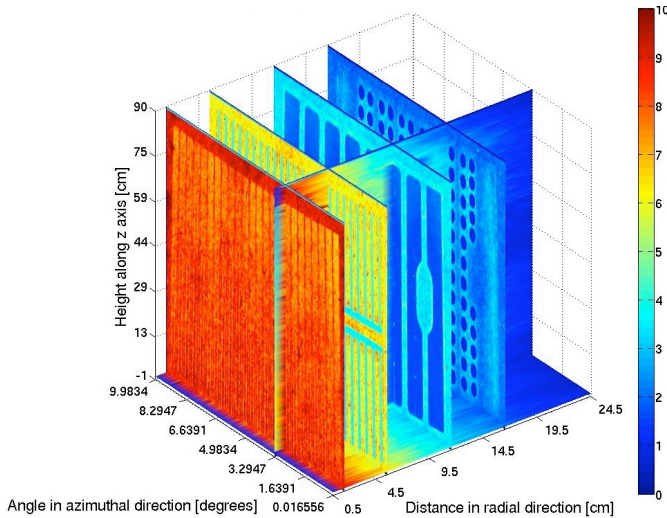


Fig. 10. 3-D visualization of nuclear heating in FWS module.

Although the radial variation generally agrees with the 1-D results, the results show that significant variations in heating and He production occur at each radial location compared to the single average value provided from the 1-D calculations. In addition, these high fidelity, high-resolution results revealed important heterogeneity effects on nuclear parameters. While at a given radial location, nuclear heating is higher in steel than in water regions, the steel nearest the water sees the highest nuclear heating because of gamma generation in the water itself and the softer neutron spectrum in SS resulting in more gamma generation. While the He production results inside the front water manifold itself are not physically meaningful, they do indicate that the neutron flux spectrum in the water regions would lead to a higher He production in steel and thus suggests that He production in the steel immediately adjacent to the water is larger than the average He production in the steel. Helium production peaking in steel at the interface with water is due to a softer neutron spectrum resulting in increased He production primarily in B-10. Another secondary contribution comes from helium production in a two-step reaction of low-energy neutrons with Ni. The SS316LN-IG used in the FWS has 10 wppm B and 12.25 wt% Ni [4]. This effect is important for re-welding considerations.

V. SUMMARY AND FUTURE WORK

Neutronics analysis was performed for ITER FWS modules 7, 12, and 13. We performed neutronics analysis to support the US design of FWS modules 7, 12 and 13. Initial 1-D and 2-D analyses were performed using homogenized radial zones for each of the FWS modules. The results were normalized to the neutron wall loading at the front of each module as determined from detailed 3-D calculations for the full ITER CAD model with the detailed source profile. Nuclear heating radial profiles were determined in each of the constituent materials. In addition, the nuclear parameters were determined at the inner surface of the VV. The impact of radiation streaming through zones with large water content, such as the water coolant manifolds and FW attachment legs, was evaluated. This results in local peaking in VV radiation parameters (nuclear heating, radiation damage, and helium production). The peaking was found to be the largest for nuclear heating that is dominated by gamma heating.

In order to preserve the significant heterogeneity of the FWS module, a hybrid 1-D/3-D neutronics analysis was performed for module 13 with all geometrical details of the module preserved. An innovative computational tool (MCNPX-CGM) for nuclear analysis that performs the neutronics calculations directly in the CAD model was used. Detailed nuclear heating, radiation damage, and helium production profiles were generated. These high fidelity, high-resolution results revealed important heterogeneity effects on nuclear parameters. Significant variations in heating and He production occur at each radial location as a result of heterogeneity while much less variation is observed in dpa. While nuclear heating is higher in steel than in water regions, the steel nearest the water sees the highest nuclear heating. In addition, He production in the steel immediately adjacent to the water is larger than the average He production in the steel.

A full 3-D analysis will be performed in which the CAD models for the FWS modules and adjacent coolant manifolds are inserted in a simplified CAD model based on a 40° sector of ITER (Fig. 2). The model includes all ITER components with suppressed details and homogenized material definitions. In addition, the accurate neutron source profile will be sampled from the exact neutron source profile provided by the ITER IO.

A thorough comparison of the results of each approximate calculation methodology to the full 3-D analysis will be used to identify the uncertainty that is inherent in such calculations. The approximate methodologies are characterized by homogenization of the materials and source distribution. While the importance of material heterogeneity has been explored in this work, the use of a uniform isotropic source in a cylindrical geometry may have important impacts on the nuclear responses calculated by the 1-D/3-D hybrid methodology near the first wall due to difference in angular distribution of source neutrons incident on the first wall.

ACKNOWLEDGMENT

This work has been performed through grants from the Sandia National Laboratories as part of DOE's funded ITER project.

References

- [1] ITER Design Description Document, 1.6 Blanket, ITER Document ITER_D_22F3M6 v2.0, August 2004.
- [2] R.E. Alcouffe, R. Baker, F. Brinkley, D. Marr, R. O'Dell, and W. Walters, "DANTSYS 3.0, A Diffusion Accelerated Neutral Particle Transport Code System, LA-12969-M, Los Alamos National Laboratory (June 1995).
- [3] D.L. Aldama and A. Trkov, "FENDL-2.1, Update of an Evaluated Nuclear Data Library for Fusion Applications," Report INDC(NDS)-467, International Atomic Energy Agency (2004).
- [4] Materials Assessment Report, Appendix B- Chemical Composition of Materials, ITER Document ITER_D_22F2PH_v.2, July 2004.
- [5] G. Federici, C. Gliss, and E. Polunovskiy, "Review of Specifications for ITER Neutronic Benchmark," Progress review meeting on procedures and tools for ITER neutronics, Madison, WI, July 24-26, 2006.
- [6] Mengkuo Wang, Douglass L. Henderson, Timothy J. Tautges, and Laila El-Guebaly, "Three-Dimensional Modeling of Complex Fusion Devices Using CAD-MCNP Interface", *Fusion Science & Technology*, vol. 47/4, pp. 1079-1083 (2005).
- [7] M. Sawan, P. Wilson, T. Tautges, L. El-Guebaly, D. Henderson, et al., "Innovative Three-Dimensional Neutronics Analyses Directly Coupled with CAD Models of Geometrically Complex Fusion Systems," Proceedings of the 13th International Conference on Emerging Nuclear Energy Systems, Istanbul, Turkey, June 3-8, 2007.
- [8] A.R. Polevoi, S. Medvedev, V. Mukhovatov, A. Kukushkin, et al., "Confinement and Stability Modelling," *J. Plasma Fusion Res. SERIES*, vol. 5, pp. 82-87 (2002).